Physical Science International Journal

Volume 26, Issue 7, Page 11-32, 2022; Article no.PSIJ.94109
ISSN: 2348-0130

Numerical Study of Turbulent Mixed Convection in a Square Lid Driven Cavity with an Inside Hot Bloc

Komlan Djiwonou Woenagnon [a], Kokou N'wuitcha [a*], Komi Apélété Amou [b] and Magolmèèna Banna [a]

[a] Laboratoire sur l'Energie Solaire, Groupe Phénomènes de Transfert et Energétique (LES-GPTE), Faculté des Sciences, Université de Lomé, 01BP: 1515, Togo.
[b] Laboratoire sur l'Energie Solaire, Chaire de l'UNESCO sur les Energies Renouvelables, Faculté des Sciences, Université de Lomé, 01BP: 1515, Togo.

Authors' contributions

This work was carried out in collaboration among all authors. All authors read and approved the final manuscript.

Article Information

DOI: 10.9734/PSIJ/2022/v26i7753

Open Peer Review History:
This journal follows the Advanced Open Peer Review policy. Identity of the Reviewers, Editor(s) and additional Reviewers, peer review comments, different versions of the manuscript, comments of the editors, etc are available here: https://www.sdiarticle5.com/review-history/94109

Original Research Article

Received: 20/09/2022
Accepted: 26/11/2022
Published: 02/12/2022

ABSTRACT

In this study, we are interested in the two-dimensional numerical simulation of the turbulent mixed convection in the case of a square with two side lid-driven cavity containing a hot obstacle. The transfer equations coupled with those of the $k-\varepsilon$ closure model and the boundary conditions were presented and discretized using the finite volume method. The coupling between the velocity and pressure fields is achieved by the SIMPLE algorithm. The technique of line-by-line scanning with the Thomas algorithm (TDMA) is used for the iterative resolution of discretized equations. The control parameters of the present study are the temperature gradient between the hot walls and the cold walls, and the speed imposed on the mobile walls. Streamlines generally show flow characterized by the presence of two counter-rotating cells. The areas adjacent to the isothermal walls and to the moving walls are the site of the development of thermal and dynamic boundary

**Corresponding author: E-mail: knwuitcha@gmail.com;*

layers, where significant temperature and velocity gradients have been observed, subsequently influencing the profiles of turbulent quantities such as turbulent viscosity, the production and dissipation of turbulent kinetic energy and the intensity of turbulence.

Keywords: Turbulent flow; mixed convection; heat transfer; lid-driven cavity; finite volume method.

NOMENCLATURES

x, y	*: Coordinates in the horizontal and vertical directions respectively (m)*
u, v	*: Average horizontal and vertical components of the velocity (m/s)*
θ	*: Temperature (K)*
k	*: Average turbulent kinetic energy (m²/s²)*
ε^*	*: Average turbulent kinetic energy dissipation (m^2/s^3)*
p	*: Average pressure (Pa)*
g	*: Gravity (m/s²)*
ρ	*: Density (kg/m^3)*
ν	*: Kinematic viscosity (m²/s)*
ν_t	*: Turbulent kinematic viscosity (m²/s)*
L	*: Length of the side of the cavity (m)*
t	*: Time (s)*

DIMENSIONLESS VARIABLES

X, Y	*: Coordinates in horizontal and vertical directions*
U, V	*: Average horizontal and vertical components of the velocity*
T	*: Average temperature*
K	*: Average turbulent kinetic energy*
P	*: Average pressure*
ν^*	*: Kinematic viscosity*
ν_t^*	*: Kinematic turbulent viscosity*
ε	*: Average turbulent kinetic energy dissipation*
T_0	*: Reference temperature*
τ	*: Time*
$\Delta\,\tau$	*: Time step*

DIMENSIONLESS NUMBERS

$V_R = \dfrac{U}{\sqrt{\dfrac{E}{\rho_s}}}$	*: Reduced velocity*
$M_A = \dfrac{\rho_f}{\rho_s}$	*: Mass number*
$C_Y = \frac{\rho_f U^2}{E}$	*: Cauchy number*
$Ri = \frac{Gr}{Re^2}$	*: Richardson number*
$Gr = \frac{g\beta\Delta T L^3}{\nu^2}$	*: Grashof number*
$Pr = \frac{\alpha}{\nu}$	*: Prandtl number*
$Re = \frac{UL}{\nu}$	*: Reynolds number*

1. INTRODUCTION

The problem of mixed convection in enclosures with moving walls is one of the main topics in the computational fluid dynamics field. The simple geometry and easy implementation of boundary conditions make it very attractive for fluid dynamics researchers to validate their numerical codes [1,2]. “The lid-driven cavity is very important for fluid flow research and is found in various engineering fields and technological applications such as flow and heat transfer in solar ponds, dynamics of lakes thermal hydraulics of nuclear reactors, food processing and float glass production" [3]. Due to its importance, a wide variety of experimental and numerical studies on lid-driven cavity flow for different configurations are available in the literature. According to Oztop et al. [4], "there are two major kinds of studies: the first one is concerned with two-dimensional enclosures where the horizontal top or bottom wall is sliding, with a constant velocity or oscillating [5,6], and similarly in three-dimensional cavities" [7,8]. "The second deals with side driven differentially heated cavities. In this case, left or right vertical wall or both vertical walls move with a constant velocity in the same or opposite in their planes. In these studies, usually the lid-driven side and the one opposing it are heated differentially to create a temperature gradient in the cavity" [9,10].

The numerical simulations of turbulent flows and heat transfer have become over the last few decades, one of the essential attentions of engineering applications in the industrial and engineering fields. Turbulence flows are mainly simulated by three methods: the Direct Numerical Simulation (DNS), the Large Eddy Simulation (LES) method and the Reynolds Averaged Navier Stokes (RANS) models" [11,12,13]. Azzouz et al. [14] "have numerically studied the two-dimensional flow in a lid driven cavity with antiparallel motion of horizontal walls both in laminar and turbulent regime for different Reynolds numbers". "In the turbulent regime, the study considered four RANS turbulence models: Omega RSM, $SST\ k\ \omega$, $RNG\ k\ \varepsilon$ and Spalart-Allmaras. The results of their studies in terms of streamline and secondary vortex depth show a high similarity of the predicted flow structures between the Omega RSM model and those from the laminar flow assumption. In contrast, the flow calculated with the SST k ω model, the $RNG\ k\ \varepsilon$ model, and the Spalart-Allmaras model reveals a remarkable underprediction that is clearly apparent in the size and number of secondary eddies in the near-wall regions" [14].

Henkes et al. [15] have investigated on "laminar and turbulent natural convection flow in a two-dimensional squared enclosure through three different turbulence models such as the standard k–ε model with logarithmic wall functions, low-Reynolds-number model of Chien [16] and low-Reynolds-number model of Jones and Launder" [17]. "Their results shown that differences between the turbulence models are largest for quantities that are determined in the inner layer of the vertical boundary layer, for instance, the wall-heat transfer and the wall-shear stress. Many researchers examined heat transmission in lid-driven cavities with a heat source inside the cavity which directly influence the flow pattern" [18–24]. "Combined mixed convective heat transfer in a lid-driven square cavity having two heats conducting spinning cylinders located inside the cavity" has been studied numerically by Paul et al. [25] They kept horizontal walls were kept adiabatic, while the right and left walls were maintained at constant higher and lower temperatures. The authors examined the combined impacts of Reynolds number and Grashoft number on the Nusselt number, concluding that Nusselt is more dependent on the increase of Grashoft than the rise of Reynolds in this particular problem.

A numerical investigation of mixed convection was conducted in a lid driven cavity with a hollow heat-conductive cylinder inside the cavity by Keya et al. [26], where the upper lid is given a constant velocity. The governing parameters of their studies were the Prandtl number, the Richardson number and the Reynolds number. The results were presented in terms of streamlines, isotherms and average heat transfer rate. They arrived to the conclusion that Richardson number has a significant impact on the flow inside the cavity, by increasing the Richardson number values, the buoyancy effect increases, and total convection and heat transfer rates improve. The flow field strength becomes more dependent on the shear force generated by lid motion as Re increases which also increases significantly heat transmission rate increases. They also observed that the fluid flow with a lower Prandtl number is more sensitive to changes in buoyancy force than fluids flow with a higher Prandtl. With rising Prandtl values, the size of the vortex grows in streamline and heat transmission is stronger at low Prandtl values than at higher Prandtl values. And finally on the basis of their results it can be observed that the flow strength increases substantially as the dimensionless time increases, and multiple vortices emerge as the convection rate increases. In the study conducted by Sin-Yeob Kim et al. [27], computational fluid dynamics analyses of buoyancy-aided turbulent mixed convection in a vertical rectangular was investigated. The CFD analyses were performed using a realisable k–ε model and a $v^2\!-f$ model and the results were compared with the experimental results constructed at Seoul National University. It was found that the results of the v^2–f model exhibited good agreement with the experimental results.

Islam et al. [18] performed the numerical investigation on laminar mixed convection characteristics in a square cavity with an isothermally heated square blockage inside has been investigated numerically using the finite volume method of the ANSYS FLUENT commercial CFD code. Various blockage ratio and the blockage position inside the cavity have been considered in this study where the blockage is maintained at a hot temperature, and the surfaces of the cavity, including the lid are maintained at à cold temperature. The governing flow parameters are the Reynolds number, the Grashof number, and the Richardson number. The flow and heat transfer behaviour in the cavity for a range of Richardson number between 0.01–100 at a fixed Reynolds number and Prandtl number is examined comprehensively. The local and the average Nusselt number at the blockage surface for different values of Richardson number and for various positions of the bloc inside the cavity. It is found that the average Nusselt number is less impacted by the value of Richardson expected when the value of the Richardson is of the order of 1 beyond which the average Nusselt number increases rapidly with the Richardson number. For the central placement of the blockage at any fixed Richardson number, the average Nusselt number decreases with increasing blockage ratio and reaches a minimum at around a blockage ratio of slightly larger than 1/2. For further increase of the blockage ratio, the average Nusselt number increases again and becomes independent of the Richardson number. The most preferable heat transfer (based on the average Nusselt number) is obtained when the blockage is placed around the top left and the bottom right corners of the cavity".

This study presents numerical analysis results on turbulent mixed convection in a double-sided lid driven cavity with a hot bloc inside the cavity, using the $k-\varepsilon$ model, and a discussion of the heat-transfer and the different turbulent some parameters predicted by the $k-\varepsilon$ models.

2. NUMERICAL SIMULATION

2.1 Problem Description

The problem under consideration is a two-sided lid driven square cavity with an isothermal hot square block inside as shown in Fig.1. The space between the bloc and the cavity is fulfilled with air which is assumed to be incompressible. The vertical walls are isothermal, maintained at cold temperature and with antiparallel motion. The lower wall is assumed to be perfectly adiabatic, and static with the no-slip boundary condition. The upper wall is static with the no-slip boundary condition. It is divided into three parts; where the central isothermal part is kept at the hot temperature and the other two parts are adiabatic. Two different cases were considered in the present study. In the first case, with the cold temperature and the velocity of the moving walls fixed, the hot temperature is gradually increased and the impact of the increase of the thermal gradient on the flow is analyzed. In the second case, the hot and cold temperatures are fixed and the impact of the increase of the moving wall velocity on the flow is studied.

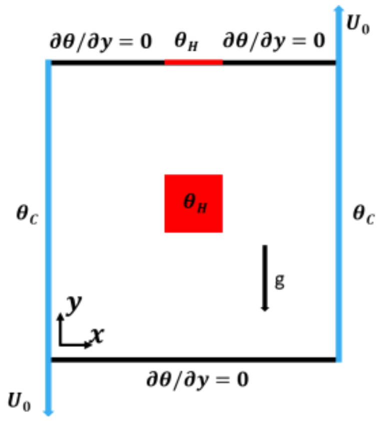

Fig. 1. Schematic diagram of the problem with boundary conditions

2.2 Governing Equations

2.2.1 Dimensional form of transfer equations

The flow is considered unsteady, turbulent, incompressible, and two-dimensional. The fluid properties are assumed to be constant except for the density variation which is modelled according to the Boussinesq approximation while viscous dissipation effects are considered to be negligible. According to the aforementioned assumptions, the governing equations for the mass, momentum, energy conservation and the standard $k-\varepsilon$ turbulence model equations are given as follows [28-31]:

- Continuity equation:

$$\frac{\partial u}{\partial x} + \frac{\partial v}{\partial y} = 0 \quad (1)$$

- Momentum equation in x direction

$$\frac{\partial u}{\partial t}+\frac{\partial}{\partial x}(uu)+\frac{\partial}{\partial y}(vu)=-\frac{1}{\rho_0}\frac{\partial}{\partial x}\left(p+\frac{2}{3}\rho_0 k\right)+\frac{\partial}{\partial x}\left[2(\nu+\nu_t)\left(\frac{\partial u}{\partial x}\right)\right]+\frac{\partial}{\partial y}\left[(\nu+\nu_t)\left(\frac{\partial u}{\partial y}+\frac{\partial v}{\partial x}\right)\right] \tag{2}$$

- Momentum equation in y direction

$$\frac{\partial v}{\partial t}+\frac{\partial}{\partial x}(uv)+\frac{\partial}{\partial y}(vv)=-\frac{1}{\rho_0}\frac{\partial}{\partial y}\left(p+\frac{2}{3}\rho_0 k\right)+\frac{\partial}{\partial x}\left[(\nu+\nu_t)\left(\frac{\partial u}{\partial y}+\frac{\partial v}{\partial x}\right)\right]+\frac{\partial}{\partial y}\left[2(\nu+\nu_t)\left(\frac{\partial v}{\partial x}\right)\right]+\rho g\beta\left(\theta-\theta_0\right) \tag{3}$$

- Energy equation

$$\frac{\partial \theta}{\partial t}+\frac{\partial}{\partial x}(u\theta)+\frac{\partial}{\partial y}(v\theta)=\frac{\partial}{\partial x}\left[\left(\frac{\nu}{\mathrm{Pr}}+\frac{\nu_t}{\sigma_t}\right)\frac{\partial \theta}{\partial x}\right]+\frac{\partial}{\partial y}\left[\left(\frac{\nu}{\mathrm{Pr}}+\frac{\nu_t}{\sigma_t}\right)\frac{\partial \theta}{\partial y}\right] \tag{4}$$

These equations are completed by the equations of the $k-\varepsilon$ standard model:

- Turbulent kinetic energy transport equation

$$\frac{\partial k}{\partial t}+\frac{\partial}{\partial x}(uk)+\frac{\partial}{\partial y}(vk)=\frac{\partial}{\partial x}\left[\left(\nu+\frac{\nu_t}{\sigma_k}\right)\frac{\partial k}{\partial x}\right]+\frac{\partial}{\partial y}\left[\left(\nu+\frac{\nu_t}{\sigma_k}\right)\frac{\partial k}{\partial y}\right]+P_k+G_k-\varepsilon^* \tag{5}$$

- Dissipation of turbulent kinetic energy transport equation

$$\frac{\partial \varepsilon^*}{\partial t}+\frac{\partial}{\partial x}(u\varepsilon^*)+\frac{\partial}{\partial y}(v\varepsilon^*)=\frac{\partial}{\partial x}\left[\left(\nu+\frac{\nu_t}{\sigma_\varepsilon}\right)\frac{\partial \varepsilon^*}{\partial x}\right]+\frac{\partial}{\partial y}\left[\left(\nu+\frac{\nu_t}{\sigma_\varepsilon}\right)\frac{\partial \varepsilon^*}{\partial y}\right]+C_1 f_1\frac{\varepsilon^*}{k}\left(P_k+C_3 G_k\right)-C_2 f_2\frac{\varepsilon^{*2}}{k} \tag{6}$$

With :

$$\begin{cases} P_k = 2\nu_t\left[\left(\frac{\partial u}{\partial x}\right)+\left(\frac{\partial v}{\partial y}\right)\right]+\nu_t\left[\left(\frac{\partial v}{\partial x}\right)+\left(\frac{\partial u}{\partial y}\right)\right] \\ G_k = -g\beta\frac{\nu_t}{\sigma_t}\left(\frac{\partial \theta}{\partial y}\right) \end{cases} \# \tag{7}$$

$$\nu_t = C_\mu f_\mu \frac{k^2}{\varepsilon}\ ;\quad f_\mu=\exp\left(\frac{-3.4}{\left(1+\frac{\mathrm{Re}_T}{50}\right)^2}\right)\ ;\quad \mathrm{f}_1=1\ ;\quad f_2=1-0.3\exp\left(-\mathrm{Re}_T{}^2\right) \tag{8}$$

The constants of the turbulent model are defined as in Table 1.

Table 1. Values of the constants of the turbulence model

C_μ	σ_t	σ_k	σ_ϵ	C_1	C_2	C_3
0.09	1	1	1.3	1.44	1.92	0.70

2.2.2 Dimensional form of boundary and initial conditions

2.2.2.1 Boundary conditions

On the walls of the obstacle:

$$u = v = 0;\ k = 0;\ \varepsilon^* = 0;\ \theta = \theta_C \tag{9}$$

On the walls of the cavity:

- At $y = 0: u = 0; v = 0; \frac{\partial\theta}{\partial y} = 0\ ; k = 0\ ; \varepsilon^* = 0$ (10)
- At $y = L : u = 0;\ v = 0; \frac{\partial\theta}{\partial y}$ and $\theta = \theta_C$(Central part) $= 0\ ; k = 0\ ; \varepsilon^* = 0$ (11)
- At $x = 0: u = 0;\ v = u_0;\ \theta = \theta_0\ ; k = 0\ ; \varepsilon^* = 0$ (12)
- At $x = L: u = 0; v = u_0; \theta = \theta_0\ ; k = 0\ ; \varepsilon^* = 0$ (13)

2.2.2.2 Initial conditions

The initial conditions used to solve the problem are as follows:

For t = 0, $u = 0\ ; v = 0\ ; \theta = \theta_0\ ; k = 10^{-3}\ ; \varepsilon^* = 10^{-3}$ (14)

2.2.3 Non dimensional form of transfer equations

The equations, the associated initial and boundary conditions defined above are made non-dimensional by introducing the following dimensionless variables and parameters:

$$X = \frac{x}{L} \quad Y = \frac{y}{L} \quad \tau = \frac{tV_{in}}{L}$$
$$V = \frac{v}{V_{in}} \quad U = \frac{u}{V_{in}} \quad P = \frac{p - p_0}{\rho V_{in}^{\ 2}} \tag{15}$$
$$T = \frac{\theta - \theta_0}{\theta_p - \theta_0} \quad K = \frac{k}{V_{in}^{\ 2}} \quad \varepsilon = \frac{\varepsilon^* L^2}{\nu V_{in}^2}$$
$$\mathrm{Re} = \frac{V_{in} h}{\nu} \quad Gr = \frac{g\beta\left(\theta_p - \theta_0\right)h^3}{\nu^2} \quad \mathrm{Pr} = \frac{\alpha}{\nu}$$

The dimensionless equations obtained from the dimensionless variables posed above are as follows:
- Continuity equation:

$$\frac{\partial U}{\partial X} + \frac{\partial V}{\partial Y} = 0 \tag{16}$$

- Momentum equation in x direction

$$\frac{\partial U}{\partial \tau} + \frac{\partial}{\partial X}\left(UU\right) + \frac{\partial}{\partial Y}\left(VU\right) = -\frac{\partial}{\partial X}\left(P + \frac{2}{3}K\right) + \frac{h^*}{\mathrm{Re}}\frac{\partial}{\partial X}\left[2\left(1 + \nu_t^{\ *}\right)\cdot\frac{\partial U}{\partial X}\right] + \frac{h^*}{\mathrm{Re}}\frac{\partial}{\partial Y}\left[\left(1 + \nu_t^{\ *}\right)\left(\frac{\partial U}{\partial Y} + \frac{\partial V}{\partial X}\right)\right] \tag{17}$$

- Momentum equation in y direction

$$\frac{\partial V}{\partial \tau}+\frac{\partial}{\partial X}(UV)+\frac{\partial}{\partial Y}(VV)=-\frac{\partial}{\partial X}\left(P+\frac{2}{3}K\right)+\frac{h^*}{\mathrm{Re}}\frac{\partial}{\partial X}\left[\left(1+\nu_t^*\right)\left(\frac{\partial U}{\partial Y}+\frac{1}{L}\frac{\partial V}{\partial X}\right)\right]$$
$$+\frac{h^*}{\mathrm{Re}}\frac{\partial}{\partial Y}\left[2\left(1+\nu_t^*\right)\cdot\frac{\partial V}{\partial Y}\right]+\frac{1}{h^*}RiT \tag{18}$$

- Energy equation

$$\frac{\partial T}{\partial \tau}+\frac{\partial}{\partial X}(UT)+\frac{\partial}{\partial Y}(VT)=\frac{h^*}{\mathrm{Re}\,\mathrm{Pr}}\frac{\partial}{\partial X}\left[\left(1+\mathrm{Pr}\frac{\nu^*{}_t}{\sigma_t}\right)\frac{\partial T}{\partial X}\right]$$
$$+\frac{h^*}{\mathrm{Re}\,\mathrm{Pr}}\frac{\partial}{\partial Y}\left[\left(1+\mathrm{Pr}\frac{\nu^*{}_t}{\sigma_t}\right)\frac{\partial T}{\partial Y}\right] \tag{19}$$

- Turbulent kinetic energy transport equation

$$\frac{\partial K}{\partial \tau}+\frac{\partial}{\partial X}(UK)+\frac{\partial}{\partial Y}(VK)=\frac{h^*}{\mathrm{Re}}\frac{\partial}{\partial X}\left[\left(1+\frac{\nu_t^*}{\sigma_k}\right)\frac{\partial K}{\partial X}\right]+\frac{h^*}{\mathrm{Re}}\frac{\partial}{\partial Y}\left[\left(1+\frac{\nu_t^*}{\sigma_k}\right)\frac{\partial K}{\partial Y}\right]$$
$$+\frac{2h^*\nu_t^*}{\mathrm{Re}}\left[\left(\frac{\partial U}{\partial X}\right)^2+\left(\frac{\partial V}{\partial Y}\right)^2\right]+\frac{h^*\nu_t^*}{\mathrm{Re}}\left(\frac{\partial V}{\partial X}+\frac{\partial U}{\partial Y}\right)^2 \tag{20}$$
$$-\nu_t^*h^*\frac{Ri}{\mathrm{Re}}\frac{\partial T}{\partial Y}-\frac{h^*}{\mathrm{Re}}\varepsilon$$

- Dissipation of turbulent kinetic energy transport equation

$$\frac{\partial \varepsilon}{\partial \tau}+\frac{\partial}{\partial X}(U\varepsilon)+\frac{\partial}{\partial Y}(V\varepsilon)=\frac{h^*}{\mathrm{Re}}\frac{\partial}{\partial X}\left[\left(1+\frac{\nu_t^*}{\sigma_\varepsilon}\right)\frac{\partial \varepsilon}{\partial X}\right]+\frac{h^*}{\mathrm{Re}}\frac{\partial}{\partial Y}\left[\left(1+\frac{\nu_t^*}{\sigma_\varepsilon}\right)\frac{\partial \varepsilon}{\partial Y}\right]+$$
$$c_1f_1\frac{h^*}{\mathrm{Re}}\frac{\varepsilon}{K}\left\{2\nu_t^*\left[\left(\frac{\partial U}{\partial X}\right)^2+\left(\frac{\partial V}{\partial Y}\right)^2\right]+\nu_t^*\left(\frac{\partial V}{\partial X}+\frac{\partial U}{\partial Y}\right)^2-\frac{C_3\nu_t^*}{h^*\sigma_t}Ri\frac{\partial T}{\partial Y}\right\} \tag{21}$$
$$-C_2f_2\frac{h^*}{\mathrm{Re}}\frac{\varepsilon^2}{K}$$

2.2.4 Non dimensional form of boundary and initial conditions

2.2.4.1 Boundary conditions

On the walls of the obstacle

$$U=V=0;\ K=\varepsilon=0;\ \mathrm{T}=1 \tag{22}$$

On the walls of the cavity

- At $Y = 0: U = 0;\ V = 0;\ \frac{\partial T}{\partial X} = 0\ ;\ K = 0\ ;\ \varepsilon = 0$ (23)
- At $Y = 1 : U = 0;\ V = 0;\ \frac{\partial T}{\partial X} = 0$ and $T = 1$ (central part) ; $K = 0\ ;\ \varepsilon = 0$ (24)
- At $X = 0: U = 0; V = 1;\ T = 0\ ;\ K = 0\ ;\ \varepsilon = 0$ (25)
- At $X = 1: U = V = 1;\ T = 0\ ;\ K = 0\ ;\ \varepsilon = 0$ (26)

2.2.4.2 Initial conditions

The dimensionless initial conditions are as follows:

For t = 0, $U = 0\ ;\ V = 0\ ;\ \theta = \theta_0\ ;\ K = \frac{10^{-3}}{V_{in}^2};\ \varepsilon = \frac{10^{-3} * L^2}{\mathrm{v}\, V_{in}^2}$ (27)

3. NUMERICAL PROCEDURE AND VALIDATION

3.1 Numerical Procedure

The discretization procedure of the mathematical model described above is based on a finite control volume using the staggered grid arrangement. The SIMPLE algorithm is used to deal with the pressure-velocity coupling equations. The power law differencing scheme is used for the formulation of the convection contribution to the coefficients in the finite-volume equations [32]. The algebraic system resulting from numerical discretization is solved sequentially by utilizing the TDMA method [33].

The iterative procedure is used with a sub-relaxation coefficient equal to 0.8 for each dependent variables. This procedure is stopped when the following test is verified:

$\left|\frac{\phi^{n+1} - \phi^{n}}{\phi^{n+1}}\right| \le 10^{-6}$ with ϕ denoting dependent variable and n is the number of iterations.

3.2 Validation

We have tested the validity of our computational code by comparing our results with those available in the literature. To do this, we compare our results with those from the experimental work of Ampofo [34] et al on natural turbulent convection in a square cavity filled with air, on the one hand, and, on the other hand, with the results from the numerical work of Henkes et al. [35] for the case of natural turbulent convection in a square cavity fulfill with air.

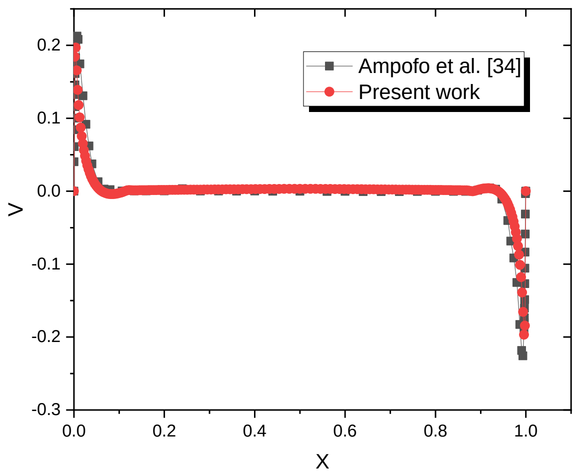

Fig. 2. Comparison of v velocity at y = 0.5

We compared quantitatively on Fig. 2 and on Fig. 3 the vertical velocity and the temperature along the vertical centerline. It is observed here that the present numerical computations match very closely those of Ampofo et al. [34]. We also qualitatively compared the flow structure, the isotherms, and the turbulent viscosity obtained by Henkes et al. [35] for the natural turbulent convection of squared cavity filled with air. As can be seen from Fig. 4, Fig. 5 and Fig. 6 there is a good agreement for the results obtained in the present study when compared to those of Henkes [35].

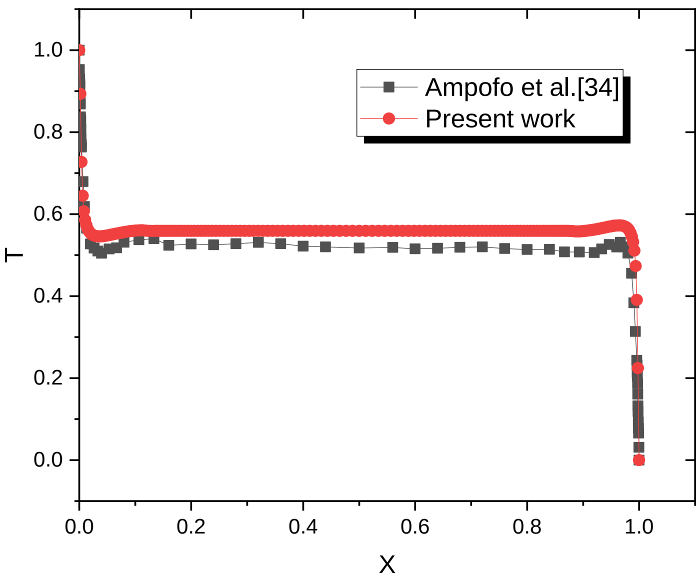

Fig. 3. Comparison of temperature at y = 0.5

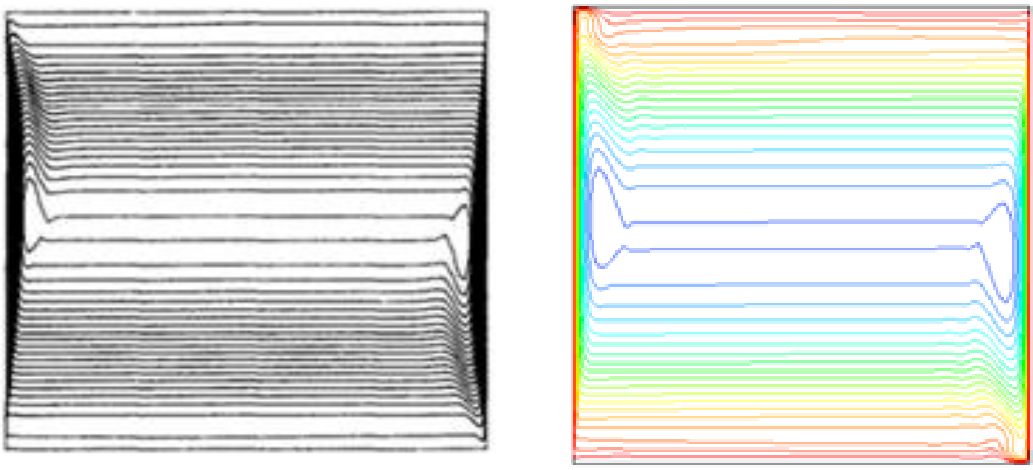

(a): Henkes et al. [35]

(b) : Present model

Fig. 4. Comparison of streamlines

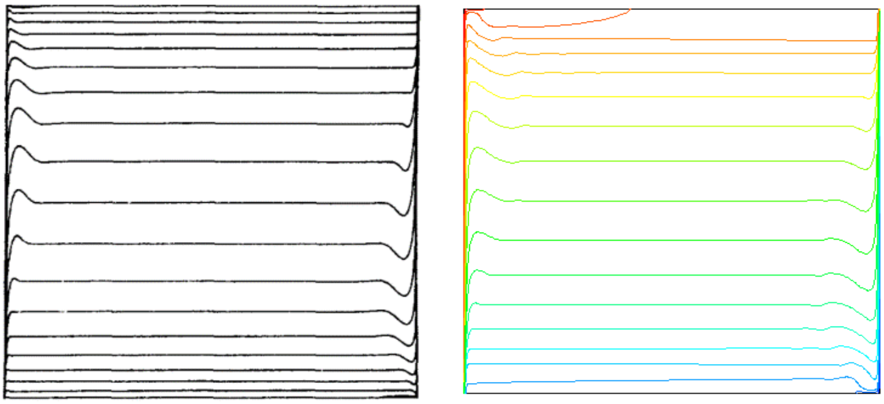

(a) : Henkes et al. [35] (b) : Present model

Fig. 5. Comparison of contour plot of temperature

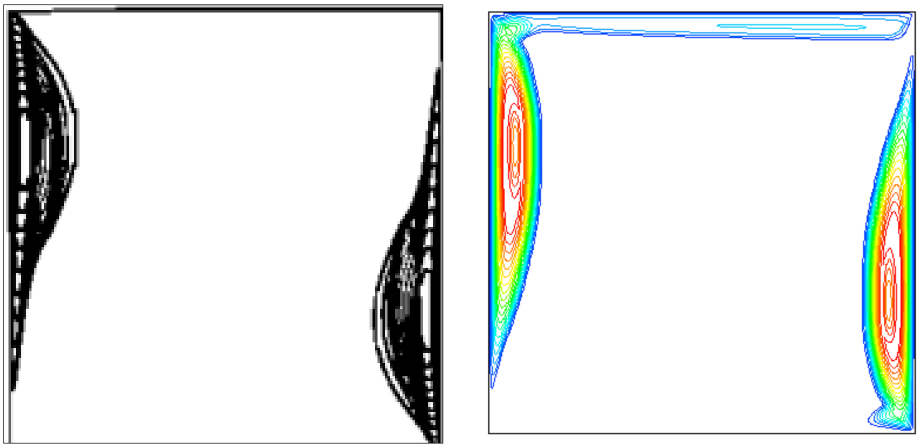

(a) : Henkes et al. [35] (b) : Present model

Fig. 6. Comparison of contour plot of turbulent viscosity

4. RESULTS AND DISCUSSION

4.1 Influence of the Thermal Gradient

The analysis done in this section show the influence of the temperature gradient between the hot and cold walls on the velocity field, the temperature field, and on turbulence characteristic parameters for a 1 m square cavity with the left wall moving downward with a velocity of $1\,m.s^{-1}$ and the right vertical wall moving upward with the same velocity in the presence of a $0.2\,m$ square obstacle. The temperature of the cold wall is maintained at $40\,°C$ and the hot temperature is increased.

4.1.1 Velocity field

For a small value of the thermal gradient ($\Delta\theta$ = 40 K), the flow structure is represented by two counter-rotating cells; one spreading from left to right throughout the lower part of the cavity at the bottom of the obstacle and the other spreading from the obstacle to the upper right corner of the cavity. These cells are deformed by the effect of the moving walls (forced convection). The highest values of velocities are observed in the cell located near the lower wall and the lowest values in the cell located on the left in the upper part. With the increase of the temperature gradient to 80 K we note that the cell in the lower part gradually disappears in favor of two large counter-rotating cells in the upper part of the cavity and two small secondary counter-rotating cells in the lower part of the cavity. At 120 K the secondary cells disappear in favor of the main cells in the upper part of the cavity, of which there is a consequent increase in their intensity and size. These cells occupy almost the entire upper part of the cavity. These different observations show that the buoyancy forces take more and more the upper part of the cavity with the birth and increase in size of the counter-rotating cells (Fig. 7). The observation of the profiles of the different components of the velocity at mid-height of the enclosure reveals that the vertical component of the velocity at this height varies very little with the increase of the temperature gradient contrary to the horizontal component which varies enormously according to the values of the thermal gradient (Fig. 8).

4.1.2 Temperature field

Looking at Fig. 9 showing the thermal fields, we notice that at low temperature gradients the heat transfer is dominated by a forced regime, and becomes mixed as the value of the thermal gradient increases. At low values of the temperature gradient, the heat transfer is more efficient because for this configuration the heat transfer depends essentially on the direction of displacement of the vertical walls. This configuration can be reproduced for industrial applications such as cooling of electronic components, thermal power plants, buildings. The temperature profiles at half height in Fig. 10 show that the temperature is constant at the surface of the obstacle with a significant increase in temperature in the vicinity of the obstacle.

4.1.3 Turbulence patterns

4.1.3.1 Turbulent kinetic energy

The turbulent kinetic energy distribution is shown in Fig. 11. It is generally noticed that the turbulent kinetic energy is more important in the vicinity of hot spots and moving walls. This is due, on the one hand, to the fluctuations of the speed of the mass of fluid entrained by the moving walls and, on the other hand, to the effect of buoyancy which causes the increase of the speed of the fluid in the vertical direction. This combined effect of natural and forced convection induces an increase in velocity fluctuations and consequently an increase in turbulent kinetic energy. The maxima are always located in the vicinity of moving walls and in the vicinity of the hot part of the upper wall. As soon as one moves away from these areas, the levels of turbulent kinetic energy are very low.

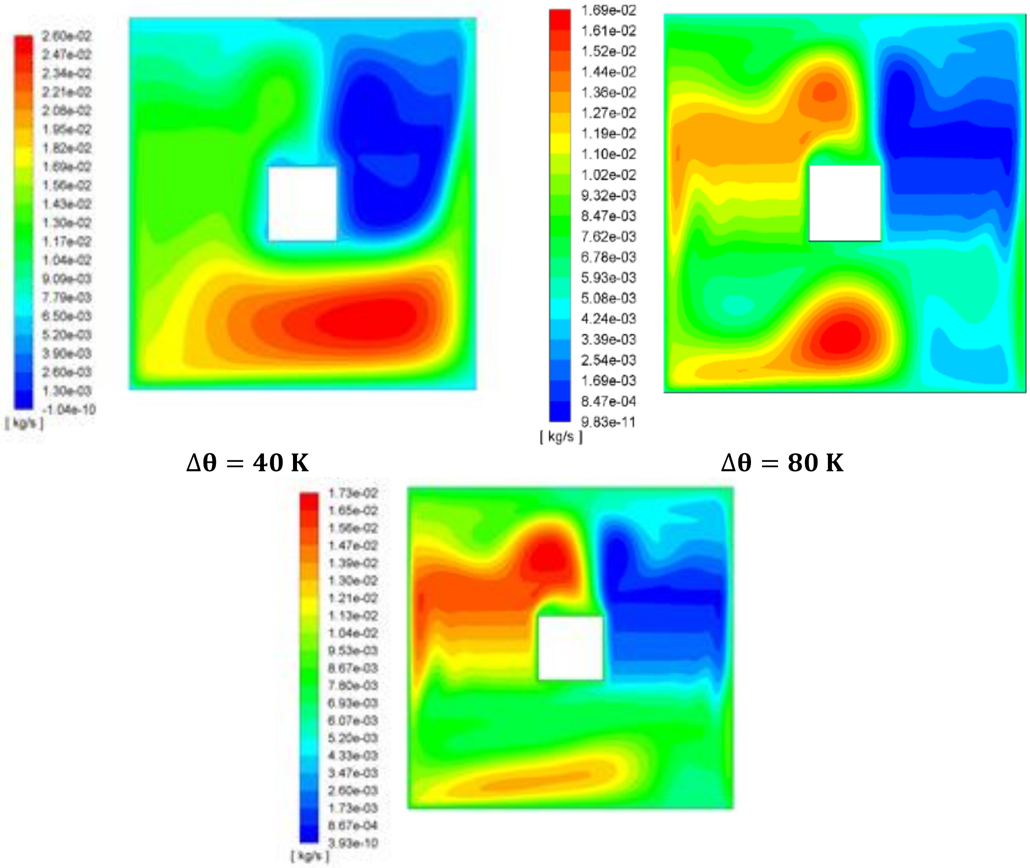

$\Delta\theta = 120$ K

Fig. 7. Streamlines for different values of the thermal gradient

The profiles of the turbulent kinetic energy at y=0.5 are shown in Fig. 12. It can be seen that the turbulent kinetic energy is higher near the moving walls; it decreases progressively when moving away from the vertical walls until it cancels. In general, it can be seen that the kinetic energy of the turbulence is higher in the areas where the current lines are more concentrated.

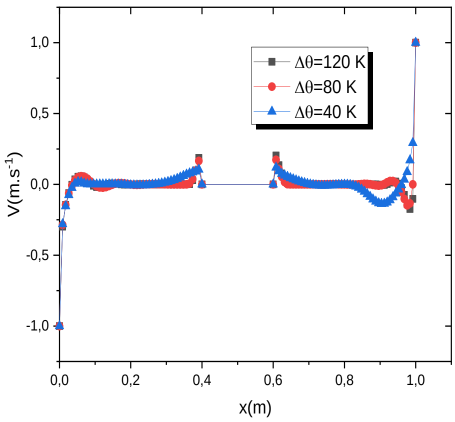

(a): v velocity profile

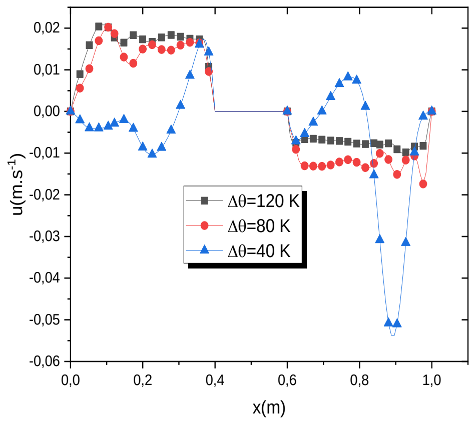

(b): u velocity profile

Fig. 8. Profiles of velocity components as a function of x for different values of the thermal gradient

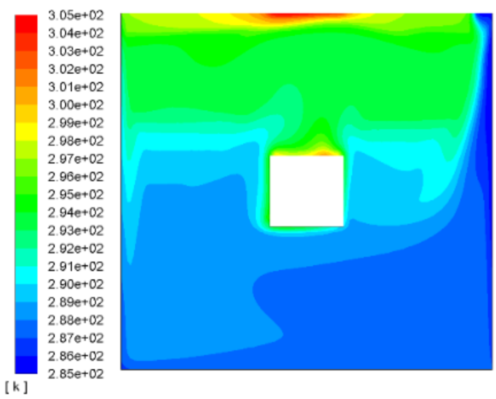

$\Delta\theta = 40$ K

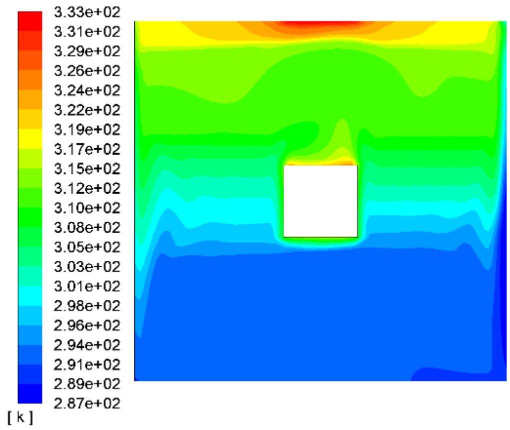

$\Delta\theta = 80$ K

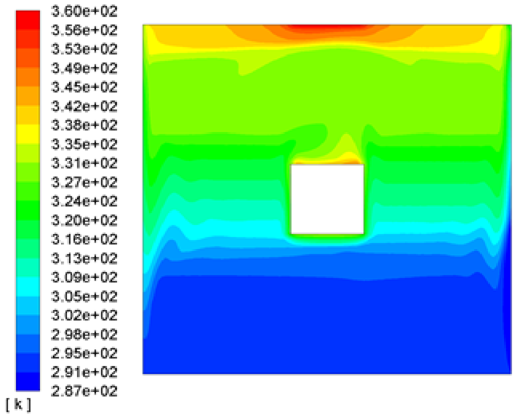

$\Delta\theta = 120$ K

Fig. 9. Isotherms for different values of the thermal gradient

4.1.3.2 Dissipation rate of the turbulent kinetic energy

The structure of the turbulent kinetic energy dissipation rate and the profiles of the turbulent kinetic energy dissipation rate at the midpoint of the enclosure are shown in Fig. 13 and Fig. 14. The same qualitative appearance is observed for the different configurations. The dissipation rate values are high in the vertical wall boundary layer which decreases sharply until they cancel. The maximum values are proportional to the thermal gradients. Away from these walls, the dissipation is zero in the rest of the cavity.

4.2 Influence of the Lid Speed

In this section we study the impact of the velocity of the vertical walls (left wall moving downward and the right wall in the opposite direction) on the fluid flow within the cavity. The temperature gradient between the hot and cold walls is kept at 60 K and the size of the square obstacle is set to 0.2 m.

4.2.1 Velocity field

Fig. 15 at V = 1 $m.\,s^{-1}$ shows us that the flow field is characterized by two large counter-rotating cells. With the increase of the velocity of the entrained walls, we notice an intensification of the convective transfers with the stratification of the streamlines around the obstacle walls modifying the structure of the flow. Indeed, for low values of the velocity imposed on the moving walls, the streamlines are affected by the movement of the walls. On the other hand, when the imposed velocity is increased, the streamlines behave almost independently of the direction of movement of the moving walls. We also notice a considerable increase in the amplitude of the flow velocity with the increase of the imposed velocity on the driven walls.

It is obvious to note that the velocity values are zero on the contours of the obstacle, as a consequence of the non-slip condition imposed on these walls and the velocity profile in the main direction of the flow (vertical direction) has negative values in the left half of the cavity and positive values in the right half with a good adherence of the boundary conditions. The flow velocity in the main direction thus follows the direction of the moving walls very well. It increases with the growth of the velocity imposed on the walls (Fig. 16).

4.2.2 Temperature field

The isotherms illustrated in Fig. 17 show a domination of the forced convection for low values of the imposed speed on the moving walls with a temperature field evolving according to the direction of movement of the walls. With the increase of the imposed velocity, the forced regime disappears progressively giving way to a mixed convection then a natural convection which settles for very high values where one observes the gradual decrease of the temperature while going from the hot points to the cold points. The profiles of temperature as function of x at the midpoint of the enclosure, shown in Fig. 18 follow the imposed conditions on temperature, with an increase in temperature as one approaches the obstacle. The temperature at the surface of the obstacle remains constant for all configurations.

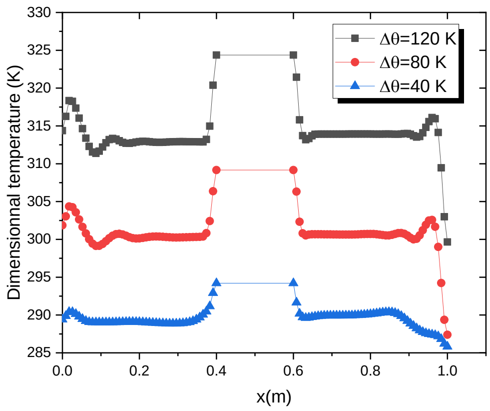

Fig. 10. Temperature profiles as a function of x for different values of the thermal gradient gradient

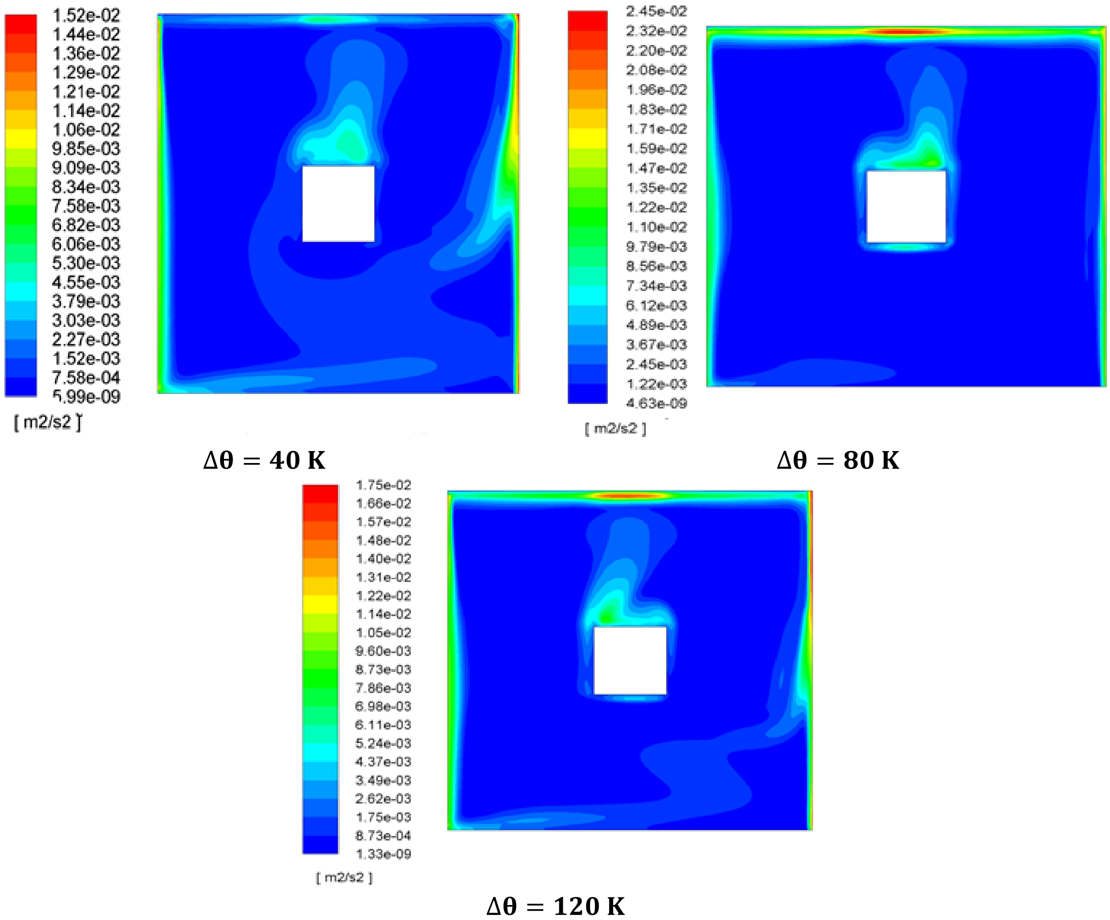

Fig. 11. Isovalues of the turbulent kinetic energy for different values thermal gradient

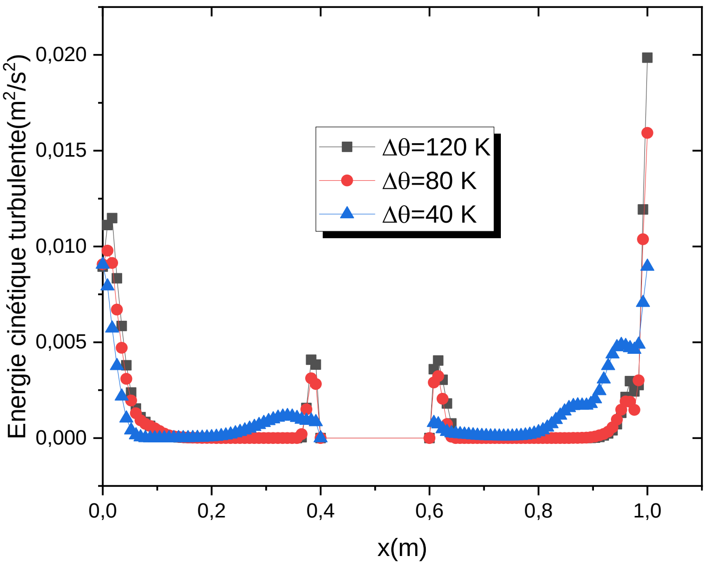

Fig. 12. Profiles of the turbulent kinetic energy as a function of x for different values of the thermal gradient

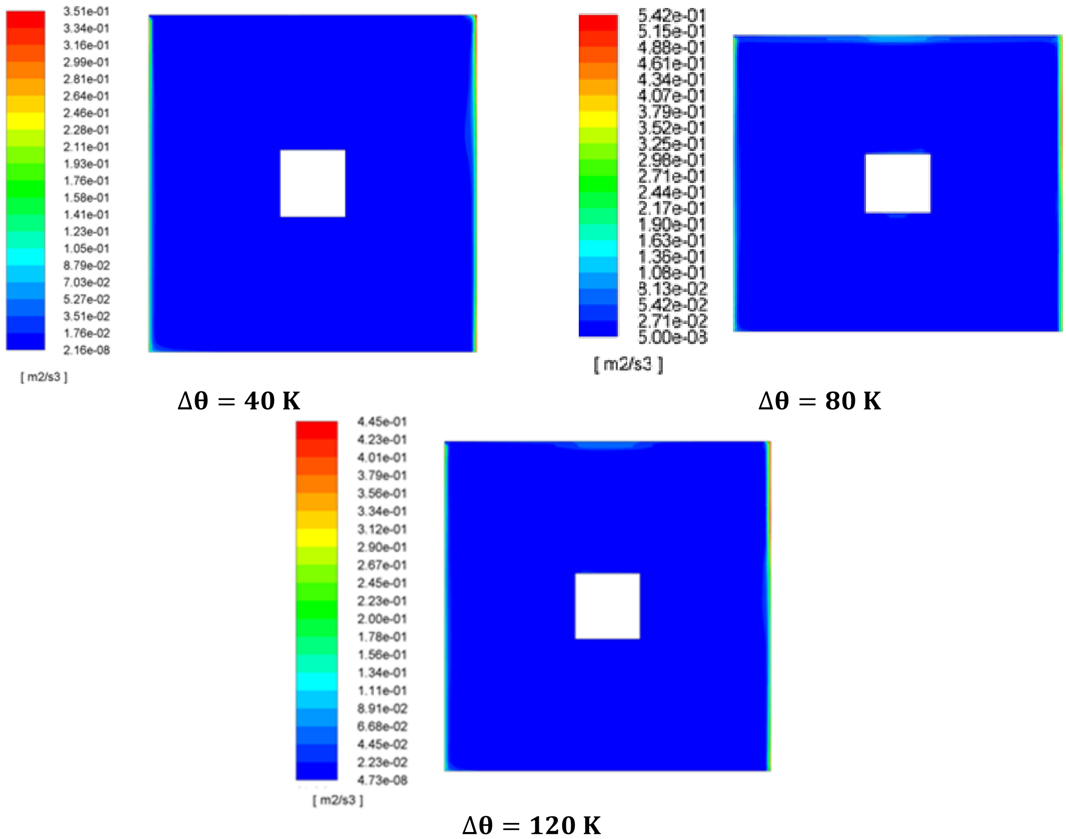

Fig. 13. Isovalues of the turbulent kinetic energy dissipation rate for different values of the thermal gradient

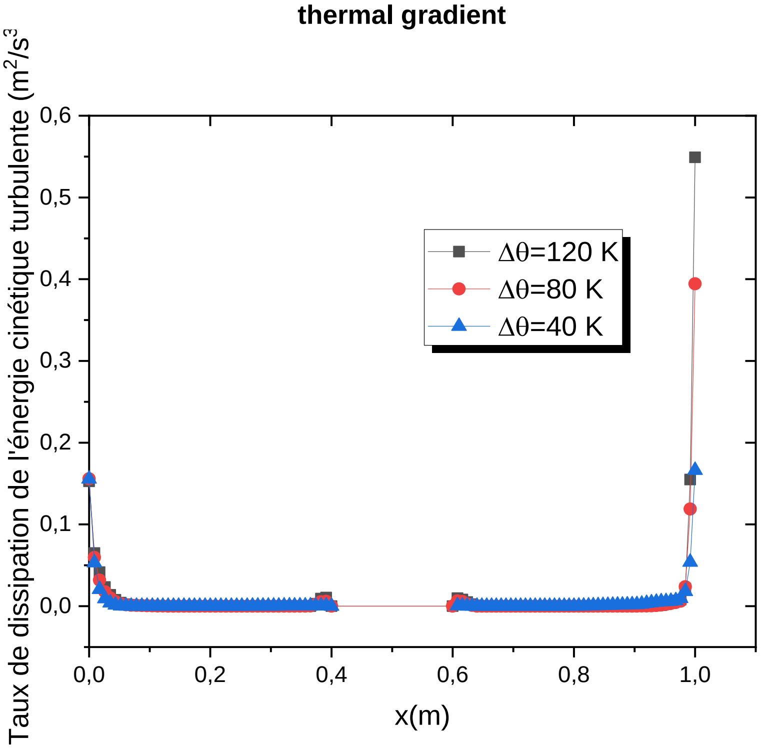

Fig.14. Profiles of the turbulent kinetic energy dissipation rate as a function of x for different values of the thermal gradient

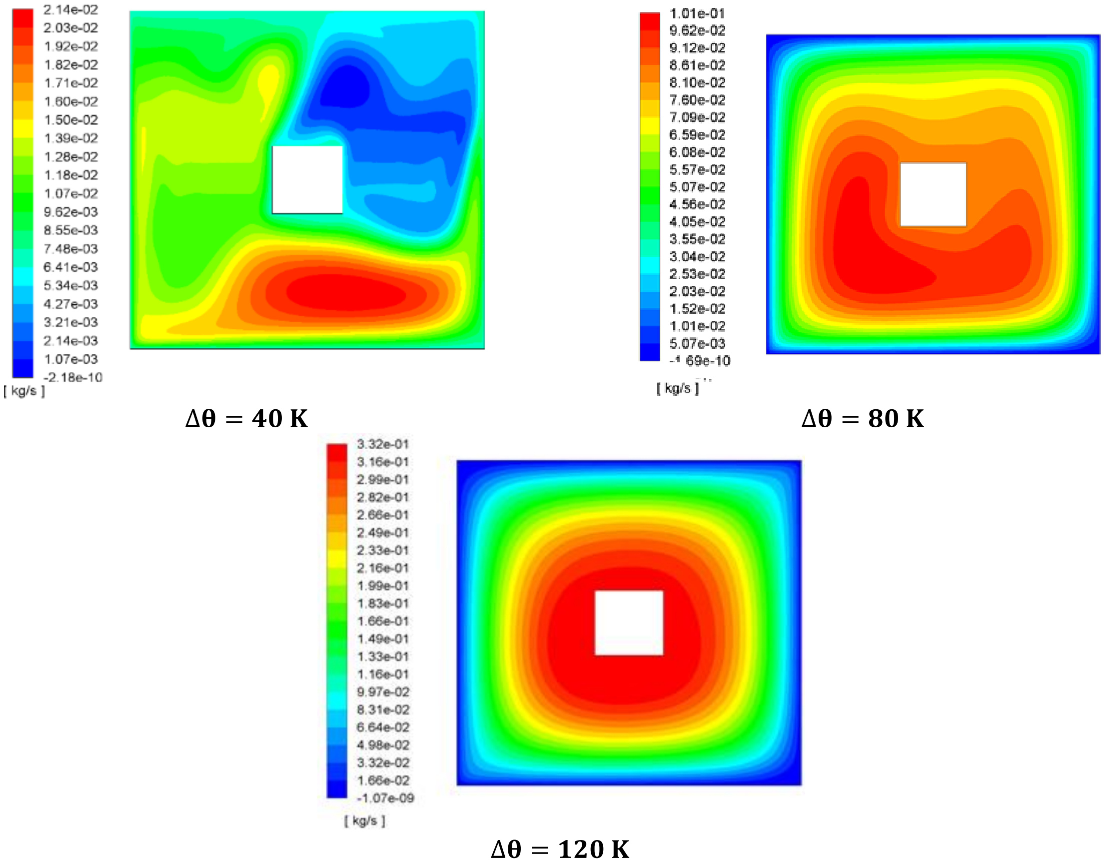

Fig. 15. Streamlines for different values of wall speed

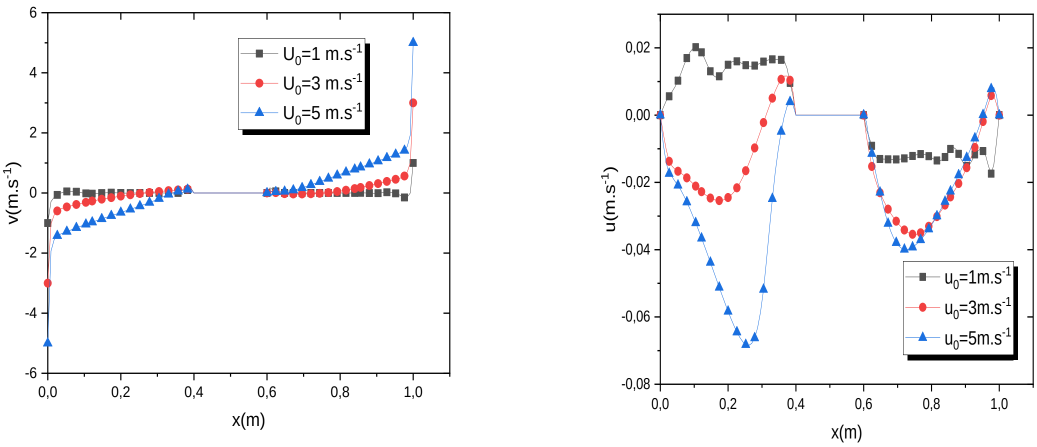

(a): v velocity profile

(b): u velocity profile

Fig. 16. Profiles of velocity components as a function of x for values of the modulus of the velocity of vertical walls in opposite directions

4.2.3 Turbulence patterns

4.2.3.1 Turbulent kinetic energy

The distribution as well as the values of the turbulent kinetic energy are strongly modified by increasing the velocity of the moving walls (Fig. 19). When the imposed velocity is $1\ m.s^{-1}$ the maximum values are recorded in the vicinity of the hot upper wall. With increasing velocity, these maxima are observed in the vicinity of the moving walls of the cavity and a gradual increase in turbulent viscosity is observed as one moves away from the obstacle and closer to the moving walls. This shows that the velocity fluctuations in the flow field are mainly caused by the kinematic condition on the vertical walls.

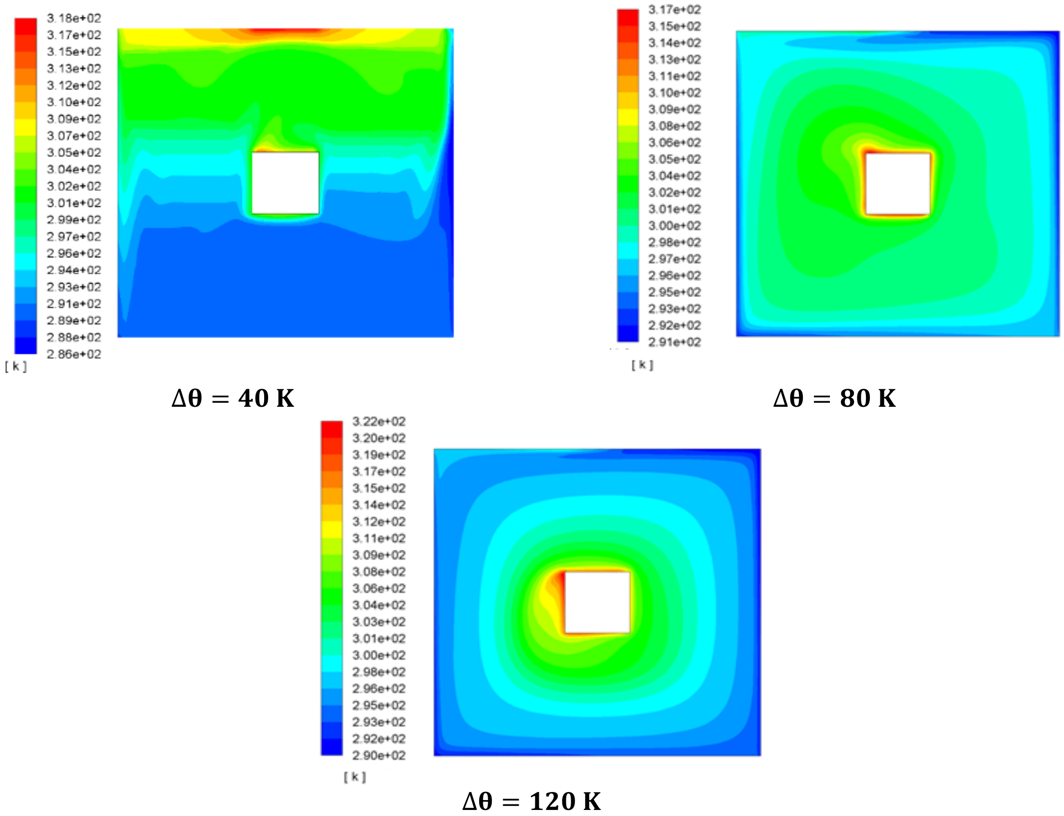

Fig. 17. Isotherms for different values of wall speed

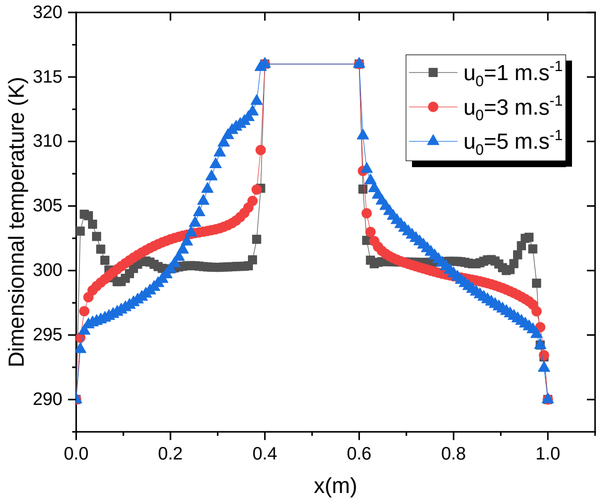

Fig. 18. Temperature profiles as a function of x for different values of the modulus of the vertical wall velocity in opposite directions

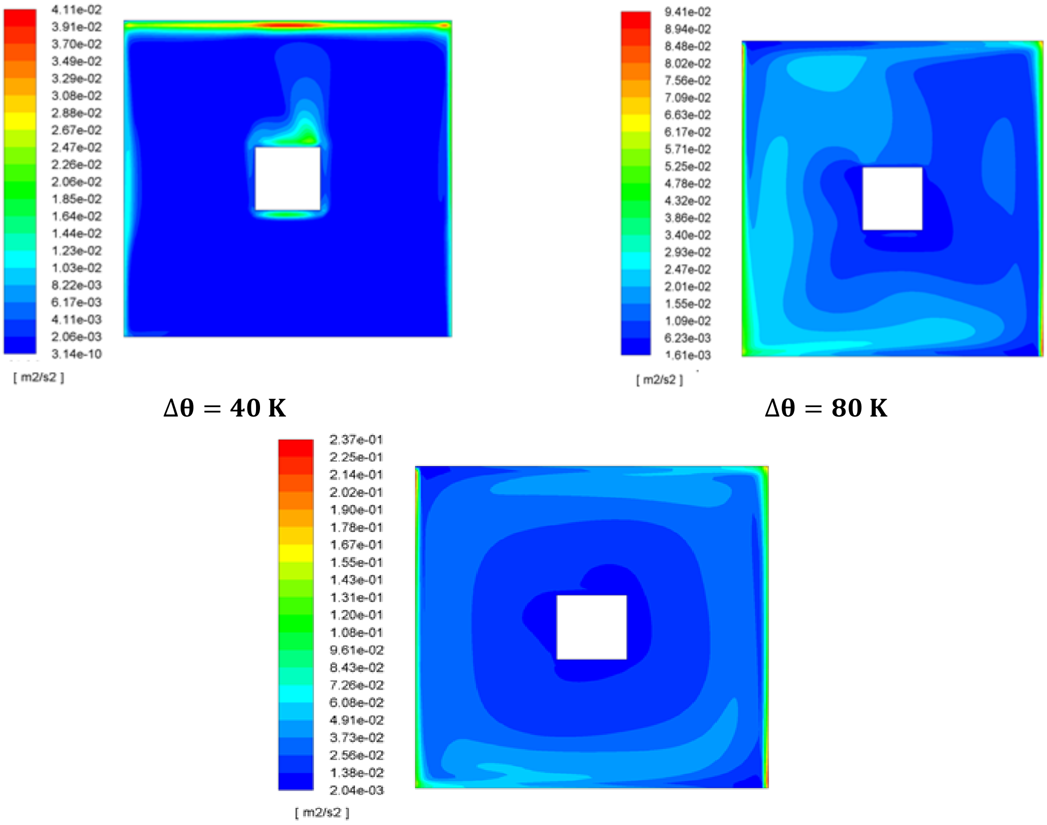

$\Delta\theta = 40$ K $\Delta\theta = 80$ K $\Delta\theta = 120$ K

Fig. 19. Isovalues of the turbulent kinetic energy for different values of the wall velocity

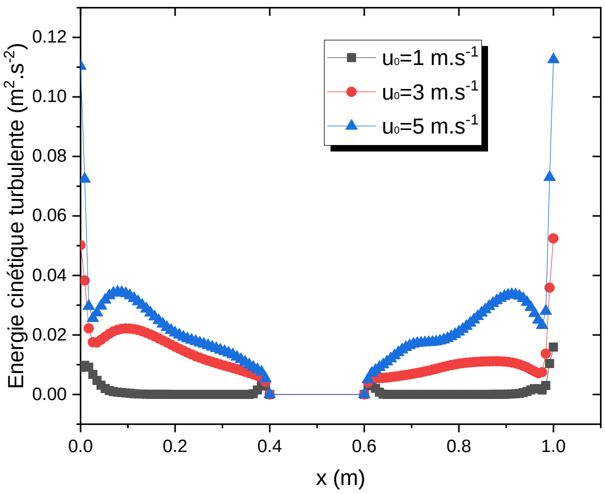

Fig. 20. Profiles of turbulent kinetic energy as a function of x for different values of the modulus of the velocity of vertical walls in opposite directions

The analysis of Fig. 20 shows us that, as for the velocity profiles at y=0.5 m the increase in the velocity of the moving walls leads to an increase in the values of the turbulent kinetic energy.

4.2.3.2 Dissipation rate of the turbulent kinetic energy

The structure of the turbulent kinetic energy dissipation rate and the profiles of the turbulent kinetic energy dissipation rate at the midpoint of the enclosure are shown in Fig. 21 and Fig. 22. The same qualitative appearance is observed for the different configurations, high values in the vertical wall boundary layer that decrease sharply until they cancel. The maximum values are proportional to the thermal gradients. Away from these walls, the dissipation is zero in the rest of the cavity.

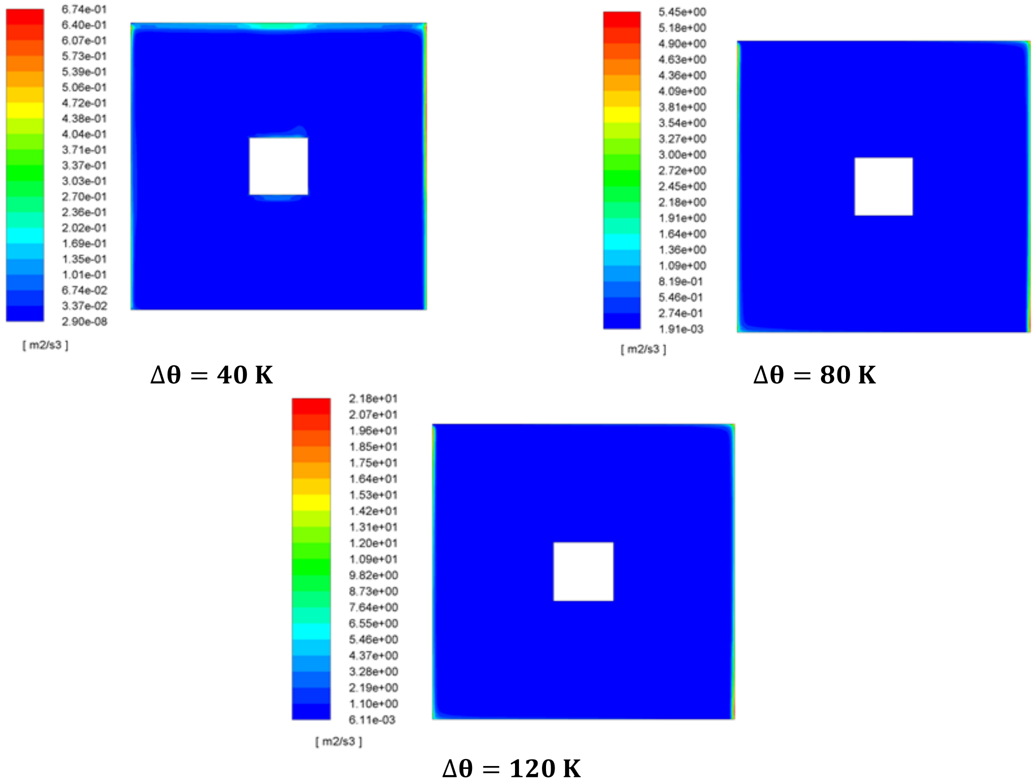

Fig. 21. Isovalues of the turbulent kinetic energy dissipation rate for different values of the wall displacement velocity

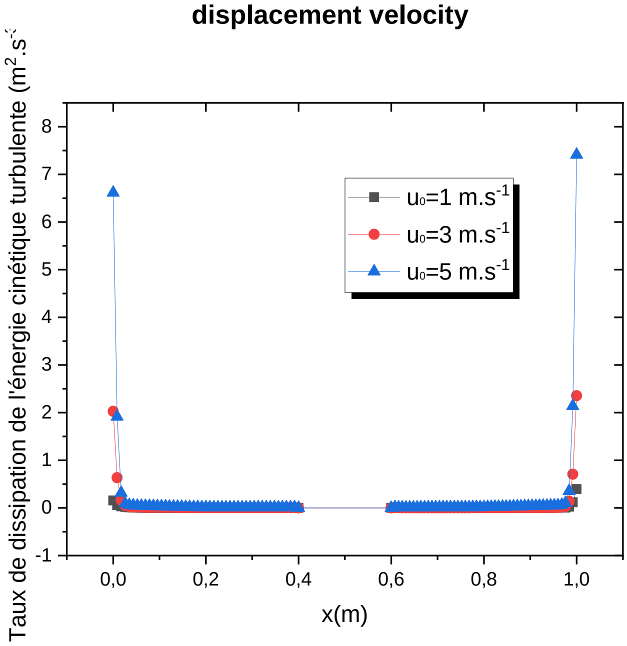

Fig. 22. Profiles of turbulent kinetic energy dissipation rate as a function of x for different values of the modulus of the vertical wall velocity in opposite directions

5. CONCLUSIONS

Turbulent mixed convection in a lid-driven square cavity having a hot square bloc inside has been investigated numerically using the $k-\varepsilon$ model, for different governing parameters. The flow parameters include the temperature gradient between the hot walls and the cold walls, and the speed imposed on the mobile walls. The streamline, the isotherm patterns, the turbulent kinetic energy pattern and the dissipation rate of the turbulent kinetic energy inside the cavity are presented for representative cases and their profile at the mid height of the cavity are plotted. Results indicate that the turbulent field is slightly affected by the temperature gradient and the velocity of the moving walls in the flow domain except along the moving wall and the heated walls where we noticed a significant variation of turbulent parameters. The temperature field changes significantly faster when increasing the temperature gradient or the speed of the moving walls. Streamlines are more affected by the increase of the velocity imposed on the moving walls than the temperature gradient. Thus, the transport of fresh fluid towards the obstacle is all the more efficient if the drag speed of the moving walls is kept low.

In the future, it would be interesting to study the fluid-structure interaction by considering the obstacle inside the cavity as deformable. This configuration has major applications in medicine, naval industry, aeronautics and civil engineering.

COMPETING INTERESTS

Authors have declared that no competing interests exist.

REFERENCES

1. Schreiber R, Keller HB. Driven cavity flows by efficient numerical techniques. J. Comput. Phys. 1983;49(2):310–333.
   DOI: 10.1016/0021-9991(83)90129-8
2. Thompson MC, Ferziger JH. An adaptive multigrid technique for the incompressible Navier-Stokes equations. J. Comput. Phys. 1989;82(1):94–121.
   DOI: 10.1016/0021-9991(89)90037-5
3. Basak T, Roy S, Sharma PK, Pop I. Analysis of mixed convection flows within a square cavity with linearly heated side wall(s). Int. J. Heat Mass Transf. 2009;52(9):2224–2242.
   DOI:10.1016/j.ijheatmasstransfer.2008.10.033
4. Oztop HF, Dagtekin I. Mixed convection in two-sided lid-driven differentially heated square cavity. Int. J. Heat Mass Transf. 2004;47(8):1761–1769.
   DOI:10.1016/j.ijheatmasstransfer.2003.10.016
5. Davis R , Eike K, Gill P, Gutman D, Hsui A, Lyons S, Zien H. Cavity flows driven by buoyancy and shear. J. Fluid Mech. 1972:51(2)221–231.
   DOI: 10.1017/S0022112072001181
6. Iwatsu R, Hyun J, Kuwahara K. Mixed convection in a driven cavity with a stable vertical temperature gradient. International Journal of Heat and Mass Transfer. 1993;36(6):1601-1608.
   DOI: 10.1016/S0017-9310(05)80069-9
7. Iwatsu R, Hyun JM. Three-dimensional driven-cavity flows with a vertical temperature gradient. Int. J. Heat Mass Transf. 1995;38(18):3319–3328.
   DOI: 10.1016/0017-9310(95)00080-S
8. Mohamad AA, Viskanta R. Flow and heat transfer in a lid-driven cavity filled with a stably stratified fluid." Appl. Math. Model. 1995;19(8):465–472.
   DOI: 10.1016/0307-904X(95)00030-N
9. Aydin O. Aiding and opposing mechanisms of mixed convection in a shear- and buoyancy-driven cavity. International Communications in Heat and Mass. 1999;26(7):1019-1028.
   DOI: 10.1016/s0735-1933(99)00091-3
10. Albensoeder S, Kuhlmann HC. Linear stability of rectangular cavity flows driven by anti-parallel motion of two facing walls. J. Fluid Mech. 2002;458:153–180.
    DOI: 10.1017/S0022112002007917
11. Lesieur M, Métais O, Comte P. Large-Eddy Simulations of Turbulence. SIAM Review; 2007.
    DOI: 10.2307/20453969
12. Nallasamy M. Turbulence models and their applications to the prediction of internal flows: A review. 1987;15(2):151-194.
    Available:https://doi.org/10.1016/S0045-7930(87)80003-8
13. Chacón Rebollo T, Lewandowski R. Mathematical and numerical foundations of turbulence models and applications. Birkhäuser; 2014th edition New York, NY: Springer; 2014.
    DOI: 10.1007/978-1-4939-0455-6
14. Azzouz EA, Houat S, Dellil AZ. Numerical assessment of turbulent flow driving in a

two-sided Lid-Driven Cavity with Antiparallel Wall motion. Defect Diffus. Forum. 2021;406:133–148.
DOI:10.4028/www.scientific.net/DDF.406.133

15. Henkes RAWM, Van Der Vlugt FF, Hoogendoorn CJ. Natural-convection flow in a square cavity calculated with low-Reynolds-number turbulence models. Int. J. Heat Mass Transf. 1991;34(2):377–388.
DOI: 10.1016/0017-9310(91)90258-G
16. Chien KY. Predictions of channel and boundary-layer flows with a low-reynolds-number turbulence model. AIAA J. 1982;20(1):33–38.
DOI: 10.2514/3.51043
17. Jones WP, Launder BE. The prediction of laminarization with a two-equation model of turbulence." Int. J. Heat Mass Transf. 1972;15(2):301–314.
DOI: 10.1016/0017-9310(72)90076-2
18. Islam AW, Sharif MAR, Carlson ES. Mixed convection in a lid driven square cavity with an isothermally heated square blockage inside. Int. J. Heat Mass Transf. 2012;55(19):5244–5255.
DOI:10.1016/j.ijheatmasstransfer.2012.05.032
19. Azizul FM, Alsabery AI, Hashim I. Heatlines visualisation of mixed convection flow in a wavy heated cavity filled with nanofluids and having an inner solid block. Int. J. Mech. Sci. 2020;175:105529.
DOI: 10.1016/j.ijmecsci.2020.105529
20. Alsabery AI, Ismael MA, Chamkha AJ, Hashim I. Effects of two-phase nanofluid model on MHD mixed convection in a lid-driven cavity in the presence of conductive inner block and corner heater. J. Therm. Anal. Calorim. 2019;135(1):729–750.
DOI: 10.1007/s10973-018-7377-6
21. Gangawane KM, Oztop HF, Ali ME. Mixed convection in a lid-driven cavity containing triangular block with constant heat flux: Effect of location of block. Int. J. Mech. Sci. 2019;152:492–511.
DOI: 10.1016/j.ijmecsci.2019.01.020
22. Ishak MS, Alsabery AI, Hashim I, Chamkha AJ. Entropy production and mixed convection within trapezoidal cavity having nanofluids and localised solid cylinder. Sci. Rep. 2021;11(1).
DOI: 10.1038/s41598-021-94238-w
23. Belarche L, Abourida B, Doghmi H, Sannad M, Ouzaouit M. Three-dimensional simulation of controlled cooling of electronic component by natural and mixed convection. Thermal Science. 2020;25 (00):181-181
DOI: 10.2298/tsci190508181b
24. Bondarenko DS, Sheremet MA, Oztop HF, Abu-Hamdeh N. Mixed convection heat transfer of a nanofluid in a lid-driven enclosure with two adherent porous blocks. J. Therm. Anal. Calorim. 2019; 135(2):1095–1105.
DOI: 10.1007/s10973-018-7455-9
25. Conjugate Mixed Convection in a Differentially Heated Lid-Driven Square Cavity With Rotating Cylinders. ASME 2020 International Mechanical Engineering Congress and Exposition. November 15-19, 2020, Portland, OR, USA.
DOI:10.1115/IMECE2020-23339
26. Keya ST, Yeasmin S, Rahman MM, Karim MF, Amin MR. Mixed convection heat transfer in a lid-driven enclosure with a double-pipe heat exchanger. Int. J. Thermofluids. 2022;13:100131.
DOI: 10.1016/j.ijft.2021.100131
27. Kim SY, Shin DH, Kim CS, Park GC, Cho HK. Computational fluid dynamics analysis of buoyancy-aided turbulent mixed convection inside a heated vertical rectangular duct. Prog. Nucl. Energy. 2021;137:103766.
DOI: 10.1016/j.pnucene.2021.103766
28. Versteeg HK, Malalasekera W. An introduction to computational fluid dynamics: The finite volume method. Pearson Education Limited; 2007.
29. Pope SB. Turbulent Flows. Cambridge University Press; 1st edition (October 16, 2000)
30. Wilcox DC. Turbulence Modeling for CFD. D C W Industries; 3rd edition (November 1, 2006)
31. Rodriguez S. Applied computational fluid dynamics and turbulence modeling. Springer; 1st ed. 2019 edition (December 18, 2019)
32. Patankar SV. Numerical heat transfer and fluid flow. Hemisphere Publishing Corporation; 1980.
33. Patankar SV, Spalding DB. A calculation procedure for heat, mass and momentum transfer in three-dimensional parabolic flows. Int. J. Heat Mass Transf. 1972;15(10):1787–1806.
DOI: 10.1016/0017-9310(72)90054-3

34. Ampofo F, Karayiannis TG. Experimental benchmark data for turbulent natural convection in an air filled square cavity. Int. J. Heat Mass Transf. 2003;46(19):3551–3572.
DOI: 10.1016/S0017-9310(03)00147-9

35. Henkes RAWM, Hoogendoorn CJ. Comparison exercise for computations of turbulent natural convection in enclosures. Numer. Heat Transf. Part B Fundam. 1995;28(1):59–78.
DOI: 10.1080/10407799508928821

Peer-review history:
The peer review history for this paper can be accessed here:
https://www.sdiarticle5.com/review-history/94109